ACS Catalysis

Research Article

Cite This: ACS Catal. 2019, 9, 8093−8103

pubs.acs.org/acscatalysis

Carbon Monoxide Activation on Cobalt Carbide for Fischer−Tropsch Synthesis from First-Principles Theory

Pei-Pei Chen,[†,∥] Jin-Xun Liu,[*,‡] and Wei-Xue Li[*,§]

[†]State Key Laboratory of Catalysis, Dalian Institute of Chemical Physics, Chinese Academy of Sciences, Dalian 116023, China

[‡]Department of Chemical Engineering, University of Michigan, Ann Arbor, Michigan 48109-2136, United States

[§]Hefei National Laboratory for Physical Sciences at the Microscale, Department of Chemical Physics, iChEM, CAS Center for Excellence in Nanoscience, University of Science and Technology of China, Hefei 230026, China

[∥]University of Chinese Academy of Sciences, Beijing 100049, China

Supporting Information

ABSTRACT: Cobalt carbide based catalyst shows a promising activity and selectivity in the direct conversion of syngas (a mixture of carbon monoxide and hydrogen molecules) toward oxygenates and lower olefin. A mechanistic understanding of the cobalt carbide structure as well as its intrinsic reactivity under Fischer−Tropsch reaction conditions is vital but remains controversial. On the basis of *ab initio* thermodynamics and density functional theory (DFT) calculations, we study here a number of the pristine Co_2C surfaces with different orientations and compositions as well as their catalytic activity on CO direct dissociation. The corresponding phase diagram and equilibrium morphology of Co_2C under a wide range of the chemical potential of carbon are constructed. Under a higher chemical potential of carbon (carbon-rich conditions), carbon-rich surfaces like (110) and (111) facets are preferentially exposed surfaces, whereas at a lower chemical potential of carbon, the stoichiometric surfaces like (011) facet could appear. Cobalt-rich surfaces such as (101) and (010) facets could be exposed only due to the kinetics hindrance under carbon-poor or hydrogen-rich conditions where the pristine bulk carbide is thermodynamically not stable. It is found that though CO adsorbs strongly on stoichiometric and carbon-rich Co_2C surfaces, the barrier for subsequent CO direct dissociation is significantly high. The presence of the carbon vacancy could promote CO direct dissociation. However, the high energy cost to produce the carbon vacancy for instance via methanation limits its overall activity toward CO activation. Implications of the present results on the role of Co_2C in direct conversion of syngas toward oxygenates and lower olefin are discussed along with available experiments.

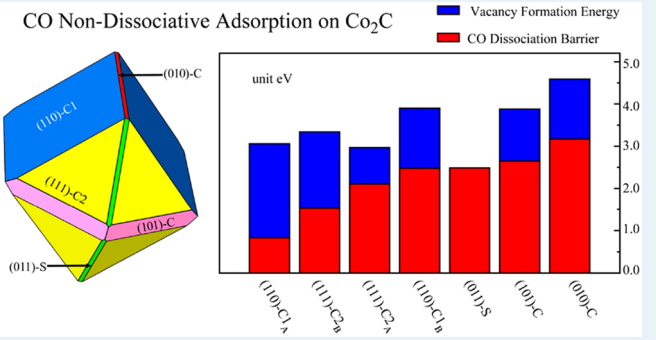

KEYWORDS: *CO dissociation, cobalt carbide, phase diagram, DFT calculation, active phase, Fischer−Tropsch synthesis*

INTRODUCTION

Fischer−Tropsch synthesis (FTS) is a leading technology that converts the syngas (mixture of carbon monoxide and hydrogen), derived from nonpetroleum feedstocks including coal, biomass, and natural gas, into valuable liquid fuels and chemicals.[1−6] Significant efforts have been devoted to enhancing the catalytic performance of the FTS catalysts toward those desirable products.[7−9] Compared to the iron-based catalysts with high selectivity toward liquid fuels or light olefins operating at relatively higher temperature,[10,11] cobalt-based catalysts have attracted more attention in recent years due to their high stability and activity toward long-chain hydrocarbon formation at lower temperature.[12−14] Co metal is recognized as the active phase for FTS, and its structure is crucial for corresponding activity and selectivity.[15−18] Co particles of a larger size are found to be more reactive than the smaller ones,[19−22] and hexagonal close-packed (hcp) Co is more reactive than face-centered cubic (fcc) Co,[23−26] due to the exposure of abundant active sites with a lower CO dissociation barrier.[27] Structure sensitivity on the crystal phase was also found in Ru recently.[28,29] A mechanistic understanding of Co-based catalysts for FTS remains essential for optimizing the catalytic activity and selectivity.

The cobalt metal can be carburized forming cobalt carbide (Co_2C) in a pure CO environment.[30−32] Under FTS conditions where both CO and hydrogen present, Co_2C was found to coexist with the Co metal.[33−35] Different from the iron carbide being the active phase for FTS, Co_2C was thought of as a sign of deactivation for FTS.[36−39] Despite its low FTS activity, the presence of Co_2C increased dramatically the

Received: February 13, 2019
Revised: July 15, 2019
Published: July 22, 2019

DOI: 10.1021/acscatal.9b00649
ACS Catal. 2019, 9, 8093−8103

selectivity of oxygenates, in particular for high alcohol synthesis (HAS).[40−44] For HAS, two distinct sites are required, primitively, one for CO associative adsorption, and one for CO dissociative adsorption and alkyl formation. It was proposed that Co_2C is responsible for the former whereas the Co metal is responsible for the latter. The intimate contact between Co_2C and Co as well as formation of the Co−Co_2C interface under FT reaction conditions were identified by transmission electron microscopy (TEM) in our earlier work.[30] Our density functional theory (DFT) calculations further showed that CO dissociation on Co_2C surfaces was unlikely due to their exceptional high dissociation barrier, whereas the coupling between alkyl formed at the Co sites and CO at the Co_2C site for alcohol is facile at the interface.[30] The same dual sites was found to increase the selectivity of hydroformylation as well.[45] Analogous synergistic interaction between Co_2C and more active components was proposed to produce selectively long-chain oxygenates, olefins, and paraffins.[46]

In addition to accommodating the sites for CO associative adsorption on Co_2C, Sun and co-workers found that when Co_2C was shaped into a nanoprism with help of Mn and Na, syngas could be converted efficiently and selectively to the lower olefin.[47−52] This is interesting since there was no cobalt metal observed by X-ray diffraction (XRD) and Transmission Electron microscopy (TEM) under FTS conditions. Accordingly, the unique morphology of Co_2C nanoprisms exposing preferentially (101) and (020) facets was proposed to be responsible for the observed selectivity. Based on DFT calculations, they proposed that CO can dissociate on the stepped Co-terminated Co_2C(020) surface.[49] At a higher reaction pressure, the Co_2C morphology was found to change from nanoprisms to nanospheres along with the appearance of the cobalt metal.[53] Accordingly, the oxygenate selectivity increases at the expense of the lower olefins.

Despite the extensive studies on Co_2C-based catalysts so far, the fundamental understanding of its intrinsic activity on syngas activation and conversion remains elusive. Actually, even for CO activation, the first step for direct conversion of syngas to oxygenates and olefin, is still controversial. Though our previous calculations found that CO dissociation on typical Co-rich and C-rich Co_2C surfaces is unlikely due to their high barriers,[30,45] CO dissociation on the stepped Co-rich Co_2C (020) surface was reported as facile.[49] Moreover, Co-rich Co_2C surfaces were used to simulate the subsequent C−C bond formation and CO insertion.[49,54,55] However, it is unclear yet, under given FT reaction conditions, which Co_2C facets are preferentially exposed and what the favorable surface compositions, for instance, Co-rich, stoichiometric, or C-rich termination, are terminated. Open and important questions remain on how the FT reaction conditions affect corresponding Co_2C facets and surface compositions exposure, and what are their intrinsic activities, for instance, in CO activation.

To address these questions, we present here an *ab initio* thermodynamics study of the phase diagram of Co_2C under a wide range of the chemical potential of carbon determined by FT reaction conditions as well as density functional theory calculations of their activity in CO direct dissociation. The remainder of the Article is organized as follows. A number of different orientated Co_2C surfaces are considered first, and favorable surface compositions at a wide range of the chemical potential of carbon are described. Wulff construction based on calculated surface free energies is used to derive the equilibrium morphology of Co_2C under three distinct chemical potentials of carbon-related FT reaction conditions. CO adsorption and direct dissociation on the exposed Co_2C surfaces derived from Wulff construction are calculated by DFT to clarify its intrinsic activity toward CO activation. The influence of surface defects, in particular, the carbon vacancy produced via methanation on CO dissociation, is addressed in detail. Finally, the implication of the present calculation with available experiments is discussed.

THEORETICAL CALCULATIONS

DFT Calculation Methods. All the spin-polarized DFT calculations were performed by using the Vienna *ab initio* simulation package (VASP)[56,57] with the projector augmented wave (PAW)[58] method for core−valence treatment. The electronic structure and energy of the ground state were calculated by using the generalized gradient approximation (GGA) with Perdew−Burke−Ernzerhof (PBE) functionals.[59] A plane-wave basis set cutoff energy of 400 eV was used. The calculated lattice constants for bulk Co_2C are a = 4.378 Å, b = 4.351 Å, and c = 2.868 Å, which are consistent with the previous experimental measurements and theoretical calculations.[30,60]

To calculate the accurate surface energy, a symmetric slab was adopted. For each surface orientation considered, different surface compositions including Co-rich, stoichiometric, and C-rich surfaces were explored. The slab thickness was approximately 20 Å separated by a vacuum of 15 Å to avoid the interactions between the neighboring slabs. The equivalent top and bottom four metallic cobalt layers (about 6 Å atomic layers thickness of C and Co atoms) were relaxed for the surface energy calculations. The electronic and force convergence limits were set to 1×10^{-5} eV and 1×10^{-2} eV/Å, respectively. The density of k-points was kept at ∼0.04 $Å^{-1}$.

A $p(2 \times 2)$ super cell with at least six metallic cobalt layers was adopted for CO adsorption and activation. CO was adsorbed on one side of the slab, and only the adsorbates and the topmost three Co and C layers were fully relaxed while the bottom layers were fixed to their bulk position. For the surface reaction calculations, the energy and force criteria for convergence were set to 1×10^{-4} eV and 0.02 eV/Å, respectively. Transition states (TSs) were determined by using the improved force reversed method,[61] and some TSs were also verified by climbing-image nudged elastic band (CI-NEB) methods;[62,63] all TSs were confirmed by frequency analysis. The reaction energies were calculated as the difference between the total energies of the products and the reactants. We chose the separate most stable adsorbed fragments on the surface as the initial and final states.

Atomistic Thermodynamics. To determine the exposed favorable surface orientation and compositions of Co_2C under FTS reaction conditions, corresponding specific Gibbs surface free energies of formation γ are calculated using *ab initio* atomistic thermodynamics[64,65]

$$\gamma = (G_{slab}(Co_{2m}C_{m+n}) - mG_{bulk}(Co_2C) - n\mu(C))/2A \quad (1)$$

where $G_{slab}(Co_{2m}C_{m+n})$, $G_{bulk}(Co_2C)$, and $\mu(C)$ are the Gibbs free energies of the carbide slab and bulk Co_2C and the chemical potential of carbon, respectively. A refers to the corresponding surface area of Co_2C surfaces in units of $Å^2$. For Co-rich, stoichiometric, and C-rich surfaces, the corresponding n is a negative, zero, and positive integer. In the present work,

DOI: 10.1021/acscatal.9b00649
ACS Catal. 2019, 9, 8093−8103

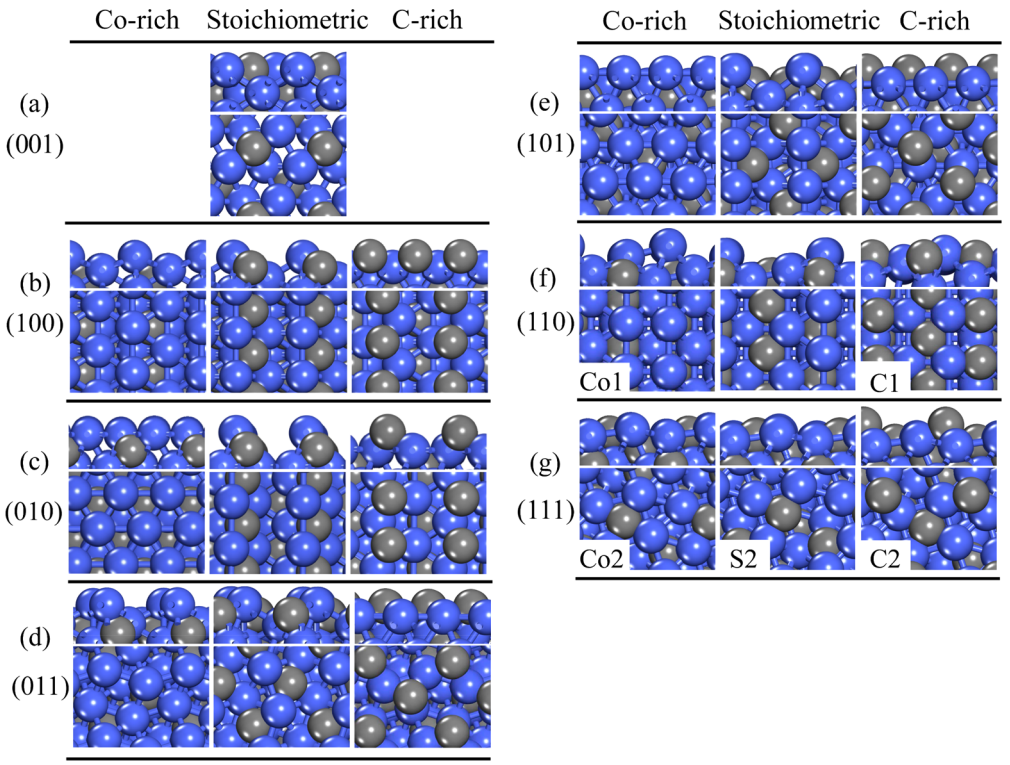

Figure 1. Schematic side and top view of Co-rich, stoichiometric, and C-rich terminated surfaces for Co_2C (001) (a), (100) (b), (010) (c), (011) (d), (101) (e), (110) (f), and (111) (g), respectively. For (110) and (111) surfaces, only the most favorable terminations from Figure 2 are shown, and the remaining surfaces are shown in Figures S1 and S2. Gray and blue spheres represent C and Co atoms, respectively. These notations are used throughout the paper.

$G_{slab}(Co_{2m}C_{m+n})$ and $G_{bulk}(Co_2C)$ were approximated by total energies $E_{slab}(Co_{2m}C_{m+n})$ and $E_{bulk}(Co_2C)$ from DFT, since the contribution of the vibrational entropy is small under considered FTS reaction conditions and because of the cancellation in part of the vibrational entropy between the carbide slab and bulk carbide.[60,66,67]

The chemical potential of carbon μ is crucial to the surface free energy and the relative stability of different orientated surfaces and surface compositions of Co_2C. At higher μ, C-rich surfaces are thermodynamically favorable, whereas at lower μ, Co-rich surfaces could become thermodynamically favorable. Under very low μ or hydrogen-rich conditions, carbon might leave cobalt carbide with the cobalt metal left if there is no kinetic hindrance, and the corresponding critical value μ_{cri} are

$$\mu_{cri}(C) = E_{bulk}(Co_2C) - 2E_{bulk}(Co) \quad (2)$$

In the present work, the calculated μ_{cri} for cobalt carbide is −8.94 eV. We note that its absolute calculated value depends on specific DFT implementation. Nevertheless, the influence of reaction conditions could be added convieniently as indicated below.

It is well-known that, under a pure H_2 environment, representing an extreme C-poor condition, the cobalt carbide would be reduced to the cobalt metal,[30,36] whereas under a pure CO environment, representing an extreme C-rich condition, the cobalt metal would be carburized to the cobalt carbide.[30−32] Under typical FTS reaction conditions, both H_2 and CO are presented at high temperatures and elevated pressure, and the corresponding μ(C) will stand in between. Whether the cobalt carbide or the cobalt metal is stable and what type of facets and surface compositions (Co-rich, stoichiometric, or C-rich) are favorable are therefore a functional of μ.

The chemical potential of carbon is a function of temperature, total pressure, H_2/CO ratio, as well as partial pressure of other hydrocarbons, H_2O and CO_2, etc.[66,68−70] Jiao and co-workers discussed μ under a broad range of FT reaction conditions.[66,68] It was found that μ decreases with increasing H_2/CO ratio. In addition to CO and H_2, μ is sensitive to the partial pressure of hydrocarbons in the gas phase: with more long-chain alkenes and alkynes (like C_2H_4 and C_2H_2), the corresponding μ is higher, whereas with more short-chain alkanes (like C_2H_6 and CH_4), the corresponding μ is lower. Jiao and co-workers found that, for temperature varying from 450 to 650 K, total pressure from 1 to 60 bar, and H_2/CO ratio from 1 to 20 with about 10% of CH_4, H_2O, and CO_2 in the gas phase, the corresponding chemical potential of carbon varies in magnitude of 0.80 eV. We therefore focus below the chemical potential of carbon varying from μ_{cri} = −8.94 eV to $\mu_{FTS} = \mu_{cri}$ + 0.80 = −8.14 eV. To see the influence of reaction conditions in a much larger phase space, we study below by allowing μ to vary from −10.0 to −7.0 eV, covering more H-rich conditions and CO-rich conditions, respectively.

RESULTS

Phase Diagram and Morphology of Cobalt Carbide. We first describe Co_2C surfaces considered, including (001), (100), (010), (101), (011), (110), and (111). Depending on the surface orientations, there are different truncated surface terminations or compositions. For the (001) surface (Figure 1a), there is only the stoichiometric surface available, whereas for (100), (010), (011), and (101), there are three possible

DOI: 10.1021/acscatal.9b00649
ACS Catal. 2019, 9, 8093−8103

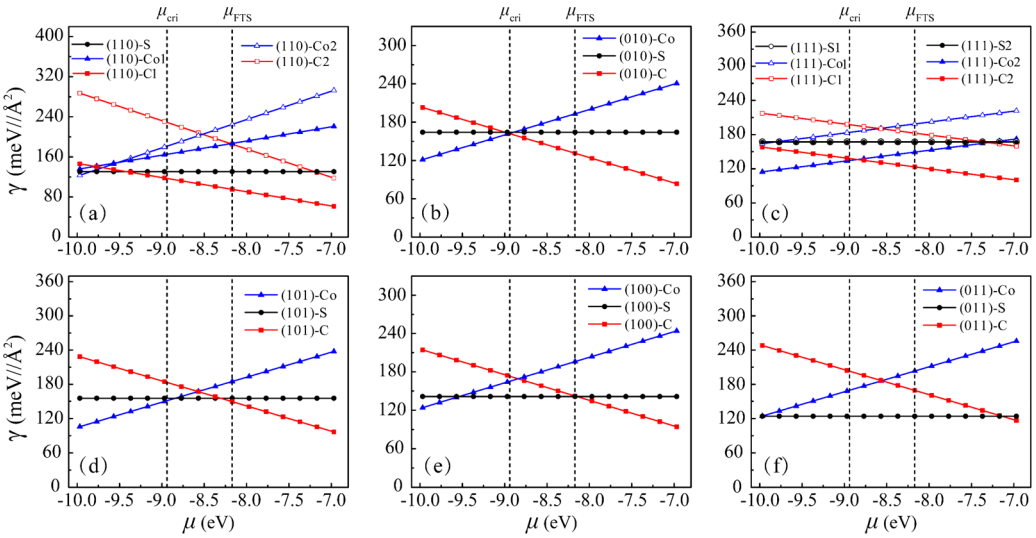

Figure 2. Surface free energy of formation γ (meV/Å^2) for various Co_2C surfaces considered as a function of the chemical potential of carbon μ. The perpendicular dashed lines $\mu_{cri} = -8.94$ eV and $\mu_{FTS} = -8.17$ eV indicate the chemical potential of carbon for the decomposition of the bulk cobalt carbide and typical FTS reaction conditions mentioned in main context.

terminations, namely, Co-rich (noted as (*hkl*)-Co afterward), stoichiometric (*hkl*)-S, and C-rich (*hkl*)-C, as shown schematically in Figure 1b−e, respectively. (110) has one stoichiometric surface, two possible C-rich surfaces (C1 and C2), and two possible Co-rich surfaces (Co1 and Co2), as shown in Figure 1f and Figures S1 and S2, respectively. For (111), there are two possible stoichiometric surfaces (S1, S2), two possible C-rich surfaces, and two possible Co-rich surfaces (Figure 1g and Figures S1 and S2). All of these surfaces were relaxed, and corresponding specific Gibbs surface free energies of formation were calculated and discussed below.

For the stoichiometric surfaces, both the Co and C atoms are exposed. According to eq 1, the resulting Gibbs surface free energy of formation γ are independent of the chemical potential of carbon ($n = 0$), as seen in Figure 2 as well. The calculated surface free energy varies from 124 to 167 meV/Å^2, depending on the surface orientation. Specifically, (011)-S has the lowest surface energy of 124 meV/Å^2, followed by (110)-S (131 meV/Å^2), (100)-S (141 meV/Å^2), (101)-S (155 meV/Å^2), (001)-S (159 meV/Å^2), and (010)-S (164 meV/Å^2). Though (111) has two possible stoichiometric surfaces, its surface free energies are the same and equal to 167 meV/Å^2. The difference in surface free energy mainly comes from their different coordination number of surface atoms and surface dipole.[60] Contrast to stoichiometric surfaces, nonstoichiometric ones depend sensitively on the chemical potential of carbon. For C-rich surfaces, irrespective of the surface orientations, the corresponding γ decreases with increasing μ due to its negative slope with respect to μ (Figure 2). Namely, the formation of C-rich surfaces is less endothermic at a higher μ and becomes more favorable with an increase of μ. For Co-rich surfaces, the corresponding γ increases with μ due to its positive slope, and the formation of corresponding surfaces is more endothermic and less favorable with an increase of μ.

For the (110) surface, Figure 2a shows that, under a wide range of μ considered, the C-rich (110)-C1 with the least γ is thermodynamically the most favorable termination as compared to the stoichiometric and Co-rich surface. For (010) surfaces, the C-rich (010)-C (Figure 2b) is the most favorable one when $\mu > \mu_{cri}$, due to its lowest γ as well. The Co-rich (010)-Co becomes favorable only when $\mu < \mu_{cri}$. A very similar result is found for the (111) surface: Co-rich surface becomes favorable only when $\mu < \mu_{cri}$, and C-rich surface becomes favorable with a further increase of μ. For (101) surfaces (Figure 2d), again Co-rich surface is favorable only when μ is less than −8.84 eV (close to $\mu_{cri} = -8.94$ eV). There is a new favorable structure, namely, stoichiometric (101)-S, occurring when -8.84 eV $< \mu < -8.31$ eV. With a further increase of μ, C-rich (101)-C becomes favorable. For (100) and (011) surfaces, the preference of the stoichiometric surface over the Co- and C-rich surfaces is extended to an even larger range of μ, as seen in Figure 2e,f, respectively. This can be rationalized on the basis of the above results, where, for instance, (011)-S has the least surface free energy of formation, among all stoichiometric surfaces considered.

The above results show that, among all surface orientations considered, Co-rich surfaces become favorable only when the corresponding chemical potential of carbon is lower than μ_{cri}. However, under this condition, the bulk cobalt carbide is already thermodynamically not stable anymore and tends to decompose to the cobalt metal if there is no kinetics hindrance. Considering that the thermodynamics equilibrium might not be approached under reaction conditions and uncertainty in calculated μ_{cri} from density functional theory, all these structures are investigated even under the chemical potential of carbon lower than the calculated μ_{cri}. In this context, we note that *in situ* experimental characterization with an atomic resolved structure and composition under FTS reaction conditions would be most useful to resolve the possible contribution of these metastable structures to the overall activity.

Wulff construction is an approach for determining the thermodynamic equilibrium shape of a crystal with fixed volume such that its total surface free energy is minimized.[71] To do so, one draws radius vector $\boldsymbol{r}_i$ perpendicular to all possible facets, and the length of the vector is proportional to the surface energy of the facet. Then, one draws planes $\boldsymbol{p}_i$ perpendicular through the tip of the radius vectors. The convex envelope of the perpendicular planes defines the corresponding crystal shape in equilibrium. For the Wulff shape of Co_2C,

DOI: 10.1021/acscatal.9b00649
ACS Catal. 2019, 9, 8093−8103

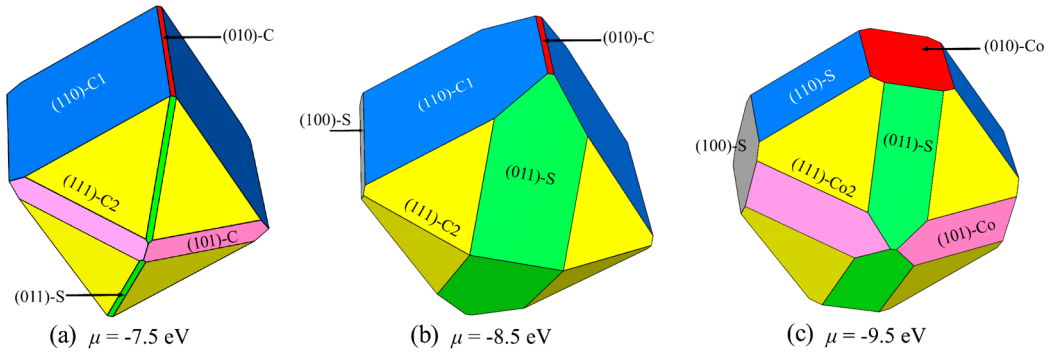

Figure 3. Equilibrium morphologies of Co_2C from the Wulff construction based on the calculated surface free energy at the chemical potential of carbon μ being −7.5 eV (a), −8.5 eV, (b) and −9.5 eV (c).

various oriented surfaces with different compositions were considered in above, and the corresponding surface free energies at different carbon chemical potential were calculated. The Wulff shapes of Co_2C were then constructed by VESTA software.[72] The Wulff construction shape tells which surface with favorable composition would be exposed and what is their exposing ratio, respectively. Since the surface free energy of Co_2C is a function of μ, the equilibrium morphology will depend on the reaction conditions as well.[68] Wulff constructions are applied here at three distinct chemical potential of carbon from high to low, and corresponding μ are −7.5 to −8.5 to −9.5 eV, and the resulting morphologies are shown in Figure 3.

For μ= − 7.5 eV (Figure 3a), it can be found that C-rich surfaces are dominating and covering about 98% of the surface area exposed. Specifically, they are (110)-C1 (60%), (111)-C2 (31%), (101)-C (6%), and (010)-C (1%). There are only 2% left occupied by the stoichiometric (011)-S surface. This is understandable since the corresponding μ represents a highly C-rich condition. By lowering μ to −8.5 eV, representing a typical FTS reaction condition (Figure 3b), the dominated (110)-C1 surface decreases from 60% to 50% and (111)-C2 from 31% to 25%, and (101)-C disappears completely. Significantly, stoichiometric (011)-S increases dramatically from 2% to 22%, and new (100)-S occurs and occupies 2%. The increase of stoichiometric surfaces at the expense of C-rich surfaces stems mainly from the surface free energies of the stoichiometric surfaces being independent of μ, whereas for the C-rich surfaces, it increases with a decrease of μ (Figure 2a,d). When reducing further the chemical potential of carbon to μ = −9.5 eV, C-rich surfaces would become even less favorable. Stoichiometric or even Co-rich surfaces become more populated. Indeed, from Figure 3c, it can be found that C-rich surfaces change to either the stoichiometric one, for instance (110)-S (21%), or even Co-rich ones, such as (111)-Co2 (34%) and (010)-Co (8%) surfaces. Moreover, new (101)-Co (13%) occurs, whereas (011)-S decreases to 16%, but (100)-S increases up to 8%. We note that again, under this condition, bulk cobalt carbide is thermodynamically not stable and tends to decompose into the cobalt metal.

CO Activation on Cobalt Carbide. We report below the CO direct activation on the surfaces exposed in the range $\mu > \mu_{cri}$ where the bulk cobalt carbide is stable and discuss the result of $\mu < \mu_{cri}$ later. CO activation is structure sensitive[27,29,73,74] and can dissociate via so-called direct (CO → C + O) and H-assisted CO dissociation (CO + H → HCO → CH + O) pathways. H-assisted CO dissociation on several selected Co-terminated and C-terminated Co_2C surfaces was addressed in our previous work.[30] We found that the corresponding barriers are comparable or even higher than those of the direct CO dissociation. A similar conclusion was also drawn on the both flat and stepped Co-terminated $Co_2C(020)$ recently.[49] These results indicate that H-assisted CO dissociation might not play a crucial role in CO dissociation on the cobalt carbide surfaces. In the present work, we thus focused on the direct CO dissociation and will address the H-assisted CO dissociation in the future. We first study the CO direct activation on two stoichiometric surfaces (100)-S and (011)-S identified. For (100)-S, CO is found to adsorb preferentially at the Co-top site (Figure 4) with an

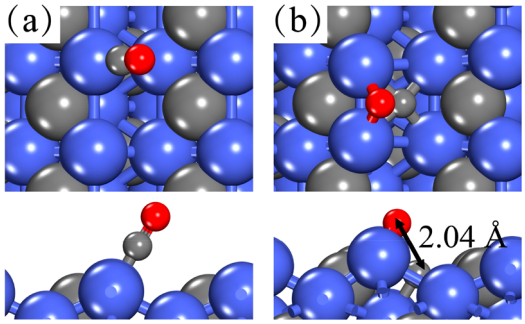

Figure 4. Top and side view of the CO adsorption configuration (a) and the transition state structure of CO dissociation on the (100)-S surface (b). The small gray and red spheres represent C and O atoms from CO, respectively.

adsorption energy of −1.85 eV. The strong adsorption can be attributed to the improved σ-donation from CO to the coordinated cationic Co atom of Co_2C.[30] Nevertheless, the barrier of the subsequent CO dissociation is as huge as 2.47 eV, since the corresponding reaction energetics are highly endothermic of 1.11 eV. The calculated CO adsorption energy on (011)-S was −1.69 eV, and the barrier of the direct dissociation is 2.49 eV, as reported in our earlier work.[45] Both stoichiometric surfaces could adsorb but not dissociate CO.

For CO direct dissociation on C-rich surfaces, our previous calculations found that corresponding barriers are higher than 2 eV.[30] This is due to the high endothermic feature of the elementary reaction energetics, derived from the pronounced electrostatic repulsion and site competition between the dissociated products and the lattice carbon. It was found that CO dissociation became facile on defected iron carbide, for instance, at the carbon vacancy.[75] We note that the carbon

DOI: 10.1021/acscatal.9b00649
ACS Catal. 2019, 9, 8093−8103

vacancy could be introduced during the synthesis or generated through hydrogenation of the lattice carbon toward hydrocarbons, for instance. We focus therefore, below, on CO adsorption and activation at the carbon vacancy of favorable C-rich surfaces, including (110)-C1, (010)-C, (111)-C2, (101)-C, (100)-C, and (011)-C, respectively. For reference, we also study (110)-C2. For (110)-C1, (110)-C2, and (111)-C2 surfaces. There are two inequivalent surface lattice carbons, labeled with A and B (Figure 5 and Figures S3 and S4), and both of them were investigated.

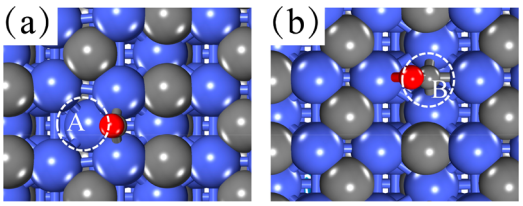

Figure 5. Top view of the CO adsorption configuration on two inequivalent carbon vacancy sites of the Co_2C(110)-C1 surface: A site (a) and B site (b).

Since the methane is the most thermodynamic stable hydrocarbon at standard conditions, compared to the longer carbon chain,[76] the formation energy E_f of the carbon vacancy via methanation was thus studied to evaluate the corresponding energy cost.

The formation energy of the carbon vacancy (E_f) is calculated as the total energy difference of the formed gaseous methane and cobalt carbide surface with a carbon vacancy from the adsorbed hydrogen atoms on the perfect cobalt carbide surfaces below:

$$E_f = E(CH_4) + E_{slab}(\text{vacancy}) - E_{slab}(\text{perfect}) - 4E_{ads}(H)$$

where $E(CH_4)$, E_{slab}(vacancy), and E_{slab}(perfect) are the calculated total energies of gaseous methane and the Co_2C slab with and without the carbon vacancy, respectively. E_{ads}(H) is the hydrogen dissociative adsorption energy on the Co_2C surface.

Main energetics results are given in Table 1, and the configurations of CO adsorption and the transition state of CO dissociation are presented in Figure 6. It can be seen from Table 1 that the CO adsorption energy E_{ads} at the carbon vacancy is considerably large, varying from −1.70 to −2.21 eV for all the surfaces considered. The binding strengths of CO toward Co_2C are similar to the Co metal,[27] and both form a strong chemical bond. The CO dissociation barrier E_{act} is found to be very sensitive to the surface orientations and composition and increases dramatically from 0.83 to 3.17 eV. High structural sensitivity for CO dissociation on various C-rich surfaces considered can be rationalized by their distinct reaction energies ΔE, varying from a very exothermic energy of −1.10 eV to a considerable endothermic energy of 0.69 eV. The difference in CO dissociation reaction energy was attributed to the different activity of the carbon vacancy, as justified by the great variation of the calculated formation energy of the carbon vacancy via methanation, and specifically, E_f changes from 0.86 to 3.42 eV, depending on the surfaces considered.

Table 1. Calculated CO Adsorption Energy E_{ads}, CO Dissociation Barrier E_{act}, and Corresponding Reaction Energy ΔE at the Vacancy of the Lattice Carbon on Various C-Rich Co_2C Surfaces Considered (Energy Unit in eV)

surfaces	E_{ads} (eV)	E_{act} (eV)	ΔE (eV)	E_f (eV)
		Window I		
(110)-$C1_A$	−1.91	0.83	−1.10	2.23
(110)-$C2_B$	−1.70	0.86	−0.92	3.42
		Window II		
(111)-$C2_B$	−2.02	1.53	−0.38	1.81
(011)-C	−2.11	1.67	0.16	1.09
		Window III		
(111)-$C2_A$	−2.10	2.11	0.69	0.86
(110)-$C2_A$	−1.74	2.13	−0.33	1.26
(110)-$C1_B$	−2.02	2.48	−0.29	1.42
(100)-C	−1.96	2.57	0.13	0.90
(101)-C	−2.17	2.65	0.34	1.23
(010)-C	−2.21	3.17	0.36	1.42

To gain better insight for CO activation on defective C-rich surfaces, we divide the calculated CO dissociation barriers into three windows (Figure 7): Window I from 0.83 to 0.86 eV, Window II from 1.53 to 1.67 eV, and Window III from 2.11 to 3.17 eV, respectively. Window I includes (110)-$C1_A$ and (110)-$C2_B$ with the lowest CO dissociation barriers of 0.83 and 0.86 eV, respectively, indicating that the corresponding process is kinetically facile. From transition states (TSs) (Figure 6a,b), it can be found that the C atom adsorbs at a 4-fold or 3-fold site while the O atom adsorbs at a bridge site by sharing two or one metal atom with the dissociated C atom with a C−O bond length of 1.95 and 2.05 Å, respectively. The calculated reaction energies are −1.10 and −0.92 eV, and high exothermic energetics show that corresponding elementary processes are energetically favorable. However, the calculated formation energies of the carbon vacancy E_f are 2.20 and 3.42 eV (Table 1). Extraordinary energy costs to form the carbon vacancies imply that the corresponding equilibrium concentrations would be rather low considering that the FTS reaction temperature is typically lower than 250 °C. Therefore, although the defected (110)-$C1_A$ and (110)-$C2_B$ surfaces show a high activity toward CO dissociation at the carbon vacancy, its low concentration limits the overall activity of the corresponding surfaces.

Window II consists of (011)-C and (111)-$C2_B$ surfaces, and calculated dissociation barriers of 1.53 and 1.67 eV increase significantly (Figure 7), respectively. Corresponding TSs can be found in Figure 6c,d, where the dissociated C and O atoms share one and two surface Co atoms with a C−O bond length of 1.90 and 1.74 Å, respectively. Compared to (110)-$C1_A$ and (110)-$C2_B$ discussed above, (011)-C has a much higher dissociation barrier of 1.67 eV. This can be understood from the change of the reaction energy from pronounced exothermic to endothermic of 0.18 eV. Meanwhile, the calculated formation energy of the carbon vacancy being 1.09 eV remains considerable. For (111)-$C2_B$, the calculated CO dissociation barrier and the formation energy of the carbon vacancy are 1.53 and 1.81 eV, respectively, which both are considerably large. With these two aspects taken together, it can be concluded that the overall rates for CO dissociation on defected (011)-C and (111)-$C2_B$ surfaces are low as well.

Window III consists of six C-terminated surfaces, (111)-$C2_A$, (110)-$C2_A$, (110)-$C1_B$, (100)-C, (101)-C, and (010)-C (Figure 7 and Table 1). The calculated formation energies of the carbon vacancy vary from 0.86 to 1.42 eV. These values are modest, indicating that the carbon vacancy on these C-

DOI: 10.1021/acscatal.9b00649
ACS Catal. 2019, 9, 8093−8103

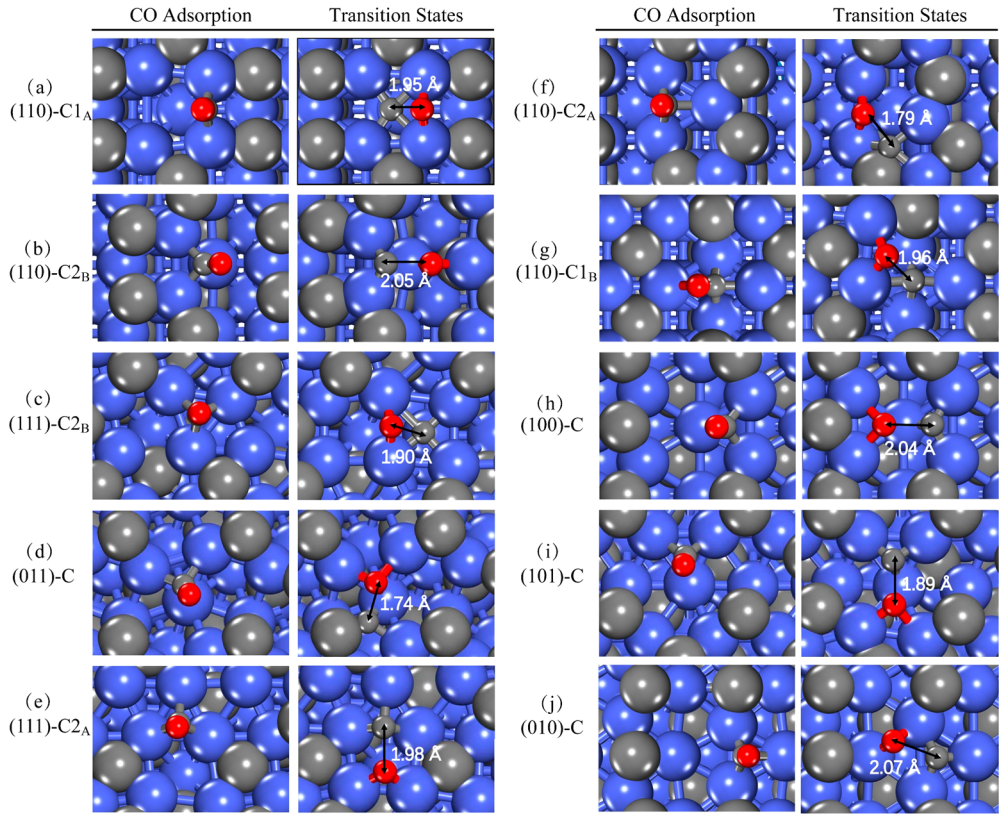

Figure 6. Schematic structures of CO adsorption and corresponding transition state of CO direct dissociation at the carbon vacancy on various C-rich Co_2C surfaces considered. The vacancy sites at A and B are illustrated in Figure 5 and Figures S3 and S4.

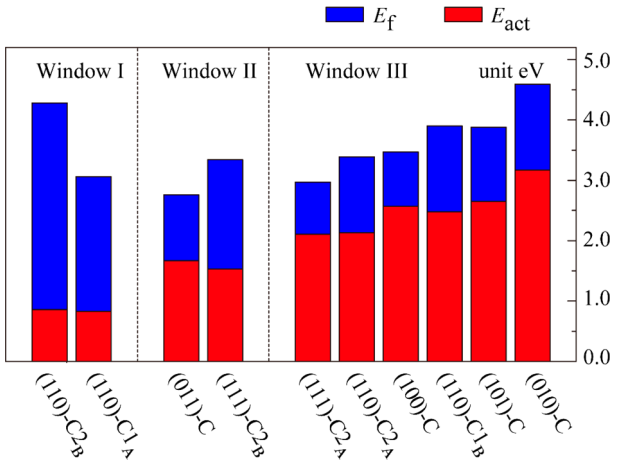

Figure 7. Calculated CO direct dissociation barriers E_{act} (red) and formation energy of lattice carbon E_f (blue) on various C-rich Co_2C surfaces considered. Units in eV.

terminated surfaces could be introduced at elvated temperatures. On the other hand, the calculated CO dissociation barriers (corresponding TSs given in Figure 6e–j) vary from 2.11 to 3.17 eV. Huge dissociation barriers would prevent the CO dissociation on these surfaces, despite high concentration of the carbon vacancies available.

It can be found from Figure 7 that the summation of the formation energy of the carbon vacancy and the CO dissociation barrier at the carbon vacancy generated, the effective barrier for CO dissociation, is more than 3 eV on all C-rich surfaces considered, irrespective of their surface orientations. This means that CO direct dissociation on C-rich surfaces hardly happens under typical FTS reaction temperature. It is interesting to note that the different carbon vacancies (labeled as A and B) on (110)-C1, (110)-C2, and (111)-C2 surfaces show very different activity for CO activation. Taking (110)-C1 (Figure 5) as an example, the calculated barriers for CO dissociation at the carbon vacancy A and B are 0.83 and 2.48 eV, respectively. The difference can refer to their distinct activity of the carbon vacancy. Specficially, the corresponding formation energy of 2.23 eV at the A sites is larger than that of 1.42 eV at the B sites, which could be rationalized by their different local coordination number (five versus four). When the cost to generate the vacancy is higher, as a compensation, there is more stabilization to the dissociated products, resulting eventually a lower dissociation barrier, which is not unexpected. The inverse correlation between the formation energy of the carbon vacancy and the CO dissociation barrier could be found referring to (110)-C2 and (111)-C2 as well.

DISCUSSION

The phase diagram presented above shows that Co-rich surfaces would be hardly exposed unless under the condition of $\mu < \mu_{cri}$, where the bulk cobalt carbide is already thermodynamically not stable. When $\mu > \mu_{cri}$, either stoichiometric or C-rich surfaces prevail. Although the proposed facets with specific composition in the Wulff shapes were not necessarily the *in situ* active surfaces under realistic FT reaction conditions because, for instance, the influence of coverage and hydrogen as well as possible kinetics limitation were not considered explicitly, our work provides a first step toward the understanding of the chemical environment

DOI: 10.1021/acscatal.9b00649
ACS Catal. 2019, 9, 8093–8103

relevant to FTS on the morphology of the cobalt carbide. For $\mu > \mu_{cri}$ where the bulk cobalt carbide remain stable DFT calculations show that corresponding pristine Co_2C surfaces exposed cannot directly dissociate CO molecules, though a strong chemical bond formed between the CO and substrate underneath, fully consistent with the experimental findings that the formation of Co_2C was considered as a sign for the deactivation of FTS.[36−39] The implication of these findings with respect to available experiments is further discussed now. We note that formation of the cobalt carbide was sensitive to the supports and the promotors,[77−82] and the same is true for the stability of the cobalt carbide as synthesized under FTS reaction conditions. Since our calculation does not consider the influence of supports and promotors, the comparison with experiments on unsupported and promotor-free Co_2C is presented first below.

Ding and co-workers synthesized unsupported and promotor-free Co_2C and performed the FTS reaction at P = 30 bar, H_2/Co = 2:1, and 220 °C.[30] In spent catalysts, considerable Co metal was found and coexisted with Co_2C to form the Co−Co_2C interface. The fact that the cobalt carbide starts to decompose under this condition indicates that the corresponding μ is already lower than μ_{cri}. Complete decomposition of Co_2C, requiring high elevated temperatures, was not observed, a fact of that should come from the kinetics hindrance and reaction dynamics. According to the above phase diagram, for $\mu < \mu_{cri}$, exposed Co_2C surfaces would be Co-rich surfaces. However, our DFT calculations found that, even on these surfaces, CO still prefers an associative rather than dissociative adsorption.[30,45] As a result, CO dissociates mainly on the fully reduced cobalt meta sites followed by C−C bond formation, the produced $C_xH_y$reacts with associative adsorbed CO from the remaining cobalt carbide sites at the Co−Co_2C interfaces to produce oxygenates.[30,35,44,45,83] In this context,we note that Davis and co-workers also found that unsupported and promotor-free Co_2C was reduced under FTS reaction conditions along with increase of the catalytic activity.[84]

It was found by Sun and co-workers[47−49,52] that Mn and Na could significantly promote the formation of Co_2C and dramatically influence the resulting morphology. Different from the Ding and Davis experiments, Co_2C nanoprisms were formed under reaction conditions of P = 1 bar, H_2/Co = 2:1, and 250 °C, and there was no metallic cobalt observed by XRD and TEM. This indicates that Mn and Na might not only promote the formation of Co_2C but also stabilize the Co_2C formed with specific morphology. Nevertheless, the detailed surface structure and composition are not available yet. According to the above calculations, irrespective of Co_2C surface orientations, CO direct dissociation on stoichiometric and C-rich surfaces hardly happens. Even on Co-rich surfaces, CO dissociation (via both the direct path and the H-assistant path) remains difficult.[30] It was reported recently that the stepped Co-terminated Co_2C (020) surface, CO could directly dissociate with a barrier of 1.34 eV.[49] We note that though the step sites were not addressed explicitly here, the present DFT calculations showed that most facets exposed in Wulff morphologies are C-rich surfaces at a wide range of the carbon chemical potentials considered. The step sites are expected to be C-rich; namely, the step sites tend to be poisoned by the carbon, which might result in a low rate for CO dissociation. How CO dissociates on Co_2C nanoprisms and forms selectively to the lower olefin requires more theoretical and experimental investigation.

Cobalt carbide in the presence of Mn and Na could be partially reduced along with morphlogy change from nanoprisms to a spheric shape when increase the total pressure from 1 to 5 bar and even higher pressure at H_2/Co = 2:1 and 230 °C. It was found that the selectivity of light olefin decreases, whereas the selectivity of higher oxygenates increase. In this particular case, the cobalt metal was not be identified by XRD yet, indicating that only the small cobalt metal particles were produced if there are any.[53] Ding and co-workers recently synthesized Mn-promoted cobalt catalysts and performed the FT reaction at P = 30 bar, H_2/CO = 2:1, and 220 °C.[35] Large amounts of the cobalt carbide were found to form and coexist with the Co metal as the reaction time progressed. Though the selectivity of the higher alcohol remains considerable, there was a pronounced increase in the selectivity of the lower olefin. These findings together with our calculation indicate that the promoters and the dual sites (the cobalt carbide and the cobalt metal), depending sensitively on the morphology and the site distribution, are essential to the selectivity and the overall activity.

CONCLUSION

Ab initio atomistic thermodynamics find that the chemical potential of carbon has a great impact on exposed surface orientations and compositions of the pristine cobalt carbide. It is found that, under the high chemical potential of carbon, C-rich surfaces, for instance Co_2C (110) and (111) surfaces are the preferentially exposed, whereas under the lowering chemical potential of carbon, considerable stoichiometric surfaces like Co_2C (011) appear. CO adsorptions on these pristine Co_2C surfaces are strongly chemically bound, whereas corresponding barriers for CO direct dissociation are significantly high. At the carbon vacancy of the C-rich surfaces, the barrier for CO direct dissociation becomes lower. However, the formation of the carbon vacancy by hydrogenation elimination (methanation) is highly demanding. It is concluded that stoichiometric and C-rich Co_2C surfaces have a rather low activity for CO direct dissociation. Co-rich surfaces like (010), (101), and (111) facets could be exposed kinetically under H-rich and/or C-poor conditions, where the pristine bulk carbide becomes thermodyanmically not stable. Further investigation of CO dissociation assisted by hydrogen on defected Co_2C surfaces, in particular, the investigation of the influence of the dual site distribution, morphology and promotors on reaction mechanism toward oxygenates and light olefin are suggested.

ASSOCIATED CONTENT

Supporting Information

The Supporting Information is available free of charge on the ACS Publications website at DOI: 10.1021/acscatal.9b00649.

Clean Co_2C(110) and (111) surfaces and two different carbon vacancy sites on Co_2C(110)-C2 and (111)-C2 (PDF)

AUTHOR INFORMATION

Corresponding Authors

*E-mail: jinxun@umich.edu.

*E-mail: wxli70@ustc.edu.cn.

ORCID

Jin-Xun Liu: 0000-0002-7499-4197

Wei-Xue Li: 0000-0002-5043-3088

DOI: 10.1021/acscatal.9b00649
ACS Catal. 2019, 9, 8093−8103

Notes

The authors declare no competing financial interest.

■ ACKNOWLEDGMENTS

We acknowledge funding from the National Key R&D Program of China (2017YFB0602205), the Natural Science Foundation of China (91645202), and the Chinese Academy of Sciences (QYZDJ-SSW-SLH054).

■ REFERENCES

(1) Khodakov, A. Y.; Chu, W.; Fongarland, P. Advances in the Development of Novel Cobalt Fischer−Tropsch Catalysts for Synthesis of Long-Chain Hydrocarbons and Clean Fuels. *Chem. Rev.* **2007**, *107*, 1692−1744.
(2) Torres Galvis, H. M.; Bitter, J. H.; Khare, C. B.; Ruitenbeek, M.; Dugulan, A. I.; De Jong, K. P. Supported Iron Nanoparticles as Catalysts for Sustainable Production of Lower Olefins. *Science* **2012**, *335*, 835−838.
(3) Spivey, J. J.; Egbebi, A. Heterogeneous catalytic synthesis of ethanol from biomass-derived syngas. *Chem. Soc. Rev.* **2007**, *36*, 1514−1528.
(4) Wang, Z.; Laddha, G.; Kanitkar, S.; Spivey, J. J. Metal organic framework-mediated synthesis of potassium-promoted cobalt-based catalysts for higher oxygenates synthesis. *Catal. Today* **2017**, *298*, 209−215.
(5) Lorito, D.; Ruocco, C.; Palma, V.; Giroir-Fendler, A.; Meunier, F. C. Reconstruction of ceria-supported Pt-Co particles under H2 and CO at 220 °C. *Appl. Catal., B* **2016**, *197*, 56−61.
(6) Yang, C.; Zhao, H.; Hou, Y.; Ma, D. Fe5C2 Nanoparticles: A Facile Bromide-Induced Synthesis and as an Active Phase for Fischer−Tropsch Synthesis. *J. Am. Chem. Soc.* **2012**, *134*, 15814−15821.
(7) Jiao, F.; Li, J.; Pan, X.; Xiao, J.; Li, H.; Ma, H.; Wei, M.; Pan, Y.; Zhou, Z.; Li, M.; Miao, S.; Li, J.; Zhu, Y.; Xiao, D.; He, T.; Yang, J.; Qi, F.; Fu, Q.; Bao, X. Selective conversion of syngas to light olefins. *Science* **2016**, *351*, 1065−1068.
(8) Cheng, K.; Gu, B.; Liu, X.; Kang, J.; Zhang, Q.; Wang, Y. Direct and Highly Selective Conversion of Synthesis Gas into Lower Olefins: Design of a Bifunctional Catalyst Combining Methanol Synthesis and Carbon−Carbon Coupling. *Angew. Chem.* **2016**, *128*, 4803−4806.
(9) Torres Galvis, H. M.; De Jong, K. P. Catalysts for Production of Lower Olefins from Synthesis Gas: A Review. *ACS Catal.* **2013**, *3*, 2130−2149.
(10) Koeken, A. C. J.; Torres Galvis, H. M.; Davidian, T.; Ruitenbeek, M.; De Jong, K. P. Suppression of Carbon Deposition in the Iron'Catalyzed Production of Lower Olefins from Synthesis Gas. *Angew. Chem.* **2012**, *124*, 7302−7305.
(11) Zhang, Q.; Kang, J.; Wang, Y. Development of Novel Catalysts for Fischer−Tropsch Synthesis: Tuning the Product Selectivity. *ChemCatChem* **2010**, *2*, 1030−1058.
(12) Sartipi, S.; Parashar, K.; Makkee, M.; Gascon, J.; Kapteijn, F. Breaking the Fischer−Tropsch synthesis selectivity: direct conversion of syngas to gasoline over hierarchical Co/H-ZSM-5 catalysts. *Catal. Sci. Technol.* **2013**, *3*, 572−575.
(13) Savost'yanov, A. P.; Yakovenko, R. E.; Narochnyi, G. B.; Bakun, V. G.; Sulima, S. I.; Yakuba, E. S.; Mitchenko, S. A. Industrial catalyst for the selective Fischer−Tropsch synthesis of long-chain hydrocarbons. *Kinet. Catal.* **2017**, *58*, 81−91.
(14) Savost'yanov, A. P.; Narochnyi, G. B.; Yakovenko, R. E.; Bakun, V. G.; Zemlyakov, N. D. Synthesis of high-molecular-weight hydrocarbons from CO and H2 over a cobalt catalyst. *Catal. Ind.* **2014**, *6*, 292−297.
(15) Iglesia, E.; Reyes, S. C.; Madon, R. J.; Soled, S. L. Selectivity Control and Catalyst Design in the Fischer−Tropsch Synthesis: Sites, Pellets, and Reactors. *Adv. Catal.* **1993**, *39*, 221−302.
(16) Weststrate, C. J.; van de Loosdrecht, J.; Niemantsverdriet, J. W. Spectroscopic insights into cobalt-catalyzed Fischer−Tropsch synthesis: A review of the carbon monoxide interaction with single crystalline surfaces of cobalt. *J. Catal.* **2016**, *342*, 1−16.
(17) Weststrate, C. J.; van Helden, P.; Niemantsverdriet, J. W. Reflections on the Fischer−Tropsch synthesis: Mechanistic issues from a surface science perspective. *Catal. Today* **2016**, *275*, 100−110.
(18) Tsakoumis, N. E.; Rønning, M.; Borg, Ø.; Rytter, E.; Holmen, A. Deactivation of cobalt based Fischer−Tropsch catalysts: A review. *Catal. Today* **2010**, *154*, 162−182.
(19) Bezemer, G. L.; Bitter, J. H.; Kuipers, H. P. C. E.; Oosterbeek, H.; Holewijn, J. E.; Xu, X.; Kapteijn, F.; Van Diilen, A. J.; De Jong, K. P. Cobalt Particle Size Effects in the Fischer−Tropsch Reaction Studied with Carbon Nanofiber Supported Catalysts. *J. Am. Chem. Soc.* **2006**, *128*, 3956−3964.
(20) Tuxen, A.; Carenco, S.; Chintapalli, M.; Chuang, C. H.; Escudero, C.; Pach, E.; Jiang, P.; Borondics, F.; Beberwyck, B.; Alivisatos, A. P.; Thornton, G.; Pong, W. F.; Guo, J.; Perez, R.; Besenbacher, F.; Salmeron, M. Size-Dependent Dissociation of Carbon Monoxide on Cobalt Nanoparticles. *J. Am. Chem. Soc.* **2013**, *135*, 2273−2278.
(21) Kitakami, O.; Sato, H.; Shimada, Y.; Sato, F.; Tanaka, M. Size effect on the crystal phase of cobalt fine particles. *Phys. Rev. B: Condens. Matter Mater. Phys.* **1997**, *56*, 13849−13854.
(22) Den Breejen, J. P.; Radstake, P. B.; Bezemer, G. L.; Bitter, J. H.; Frøseth, V.; Holmen, A.; De Jong, K. P. On the Origin of the Cobalt Particle Size Effects in Fischer−Tropsch Catalysis. *J. Am. Chem. Soc.* **2009**, *131*, 7197−7203.
(23) Ducreux, O.; Rebours, B.; Lynch, J.; Roy-Auberger, M.; Bazin, D. Microstructure of supported cobalt Fischer−Tropsch catalysts. *Oil Gas Sci. Technol.* **2009**, *64*, 49−62.
(24) Enache, D. I.; Rebours, B.; Roy-Auberger, M.; Revel, R. In Situ XRD Study of the Influence of Thermal Treatment on the Characteristics and the Catalytic Properties of Cobalt-Based Fischer−Tropsch Catalysts. *J. Catal.* **2002**, *205*, 346−353.
(25) Gnanamani, M. K.; Jacobs, G.; Shafer, W. D.; Davis, B. H. Fischer−Tropsch synthesis: Activity of metallic phases of cobalt supported on silica. *Catal. Today* **2013**, *215*, 13−17.
(26) Peña, D.; Griboval-Constant, A.; Lancelot, C.; Quijada, M.; Visez, N.; Stéphan, O.; Lecocq, V.; Diehl, F.; Khodakov, A. Y. Molecular structure and localization of carbon species in alumina supported cobalt Fischer−Tropsch catalysts in a slurry reactor. *Catal. Today* **2014**, *228*, 65−76.
(27) Liu, J. X.; Su, H. Y.; Sun, D. P.; Zhang, B. Y.; Li, W. X. Crystallographic Dependence of CO Activation on Cobalt Catalysts: HCP versus FCC. *J. Am. Chem. Soc.* **2013**, *135*, 16284−16287.
(28) Kusada, K.; Kobayashi, H.; Yamamoto, T.; Matsumura, S.; Sumi, N.; Sato, K.; Nagaoka, K.; Kubota, Y.; Kitagawa, H. Discovery of Face-Centered-Cubic Ruthenium Nanoparticles: Facile Size-Controlled Synthesis Using the Chemical Reduction Method. *J. Am. Chem. Soc.* **2013**, *135*, 5493−5496.
(29) Li, W. Z.; Liu, J. X.; Gu, J.; Zhou, W.; Yao, S. Y.; Si, R.; Guo, Y.; Su, H. Y.; Yan, C. H.; Li, W. X.; Zhang, Y. W.; Ma, D. Chemical Insights into the Design and Development of Face-Centered Cubic Ruthenium Catalysts for Fischer−Tropsch Synthesis. *J. Am. Chem. Soc.* **2017**, *139*, 2267−2276.
(30) Pei, Y. P.; Liu, J. X.; Zhao, Y. H.; Ding, Y. J.; Liu, T.; Dong, W. Da; Zhu, H. J.; Su, H. Y.; Yan, L.; Li, J. L.; Li, W. X. High Alcohols Synthesis via Fischer−Tropsch Reaction at Cobalt Metal/Carbide Interface. *ACS Catal.* **2015**, *5* (6), 3620−3624.
(31) Paterson, J.; Peacock, M.; Ferguson, E.; Purves, R.; Ojeda, M. In Situ Diffraction of Fischer−Tropsch Catalysts: Cobalt Reduction and Carbide Formation. *ChemCatChem* **2017**, *9*, 3463−3469.
(32) Karaca, H.; Safonova, O. V.; Chambrey, S.; Fongarland, P.; Roussel, P.; Griboval-Constant, A.; Lacroix, M.; Khodakov, A. Y. Structure and catalytic performance of Pt-promoted alumina-supported cobalt catalysts under realistic conditions of Fischer−Tropsch synthesis. *J. Catal.* **2011**, *277*, 14−26.
(33) Karaca, H.; Hong, J.; Fongarland, P.; Roussel, P.; Griboval-Constant, A.; Lacroix, M.; Hortmann, K.; Safonova, O. V.; Khodakov, A. Y. In situ XRD investigation of the evolution of alumina-supported

DOI: 10.1021/acscatal.9b00649
ACS Catal. 2019, 9, 8093−8103

cobalt catalysts under realistic conditions of Fischer−Tropsch synthesis. *Chem. Commun.* **2010**, *46*, 788−790.
(34) Kwak, G.; Woo, M. H.; Kang, S. C.; Park, H. G.; Lee, Y. J.; Jun, K. W.; Ha, K. S. In situ monitoring during the transition of cobalt carbide to metal state and its application as Fischer−Tropsch catalyst in slurry phase. *J. Catal.* **2013**, *307*, 27−36.
(35) Zhao, Z.; Lu, W.; Yang, R.; Zhu, H.; Dong, W.; Sun, F.; Jiang, Z.; Lyu, Y.; Liu, T.; Du, H.; Ding, Y. Insight into the Formation of Co@Co2C Catalysts for Direct Synthesis of Higher Alcohols and Olefins from Syngas. *ACS Catal.* **2018**, *8*, 228−241.
(36) Weller, S.; Hofer, L. J. E.; Anderson, R. B. The Role of Bulk Cobalt Carbide in the Fischer−Tropsch Synthesis. *J. Am. Chem. Soc.* **1948**, *70*, 799−801.
(37) Cheng, J.; Hu, P.; Ellis, P.; French, S.; Kelly, G.; Lok, C. M. Density Functional Theory Study of Iron and Cobalt Carbides for Fischer−Tropsch Synthesis. *J. Phys. Chem. C* **2010**, *114*, 1085−1093.
(38) Sadeqzadeh, M.; Karaca, H.; Safonova, O. V.; Fongarland, P.; Chambrey, S.; Roussel, P.; Griboval-Constant, A.; Lacroix, M.; Curulla-Ferré, D.; Luck, F.; Khodakov, A. Y. Identification of the active species in the working alumina-supported cobalt catalyst under various conditions of Fischer−Tropsch synthesis. *Catal. Today* **2011**, *164*, 62−67.
(39) Ducreux, O.; Lynch, J.; Rebours, B.; Roy, M.; Chaumette, P. In Situ Characterisation of Cobalt Based Fischer−Tropsch Catalysts: A New Approach to the Active Phase. *Stud. Surf. Sci. Catal.* **1998**, *119*, 125−130.
(40) Volkova, G. G.; Yurieva, T. M.; Plyasova, L. M.; Naumova, M. I.; Zaikovskii, V. I. Role of the Cu−Co alloy and cobalt carbide in higher alcohol synthesis. *J. Mol. Catal. A: Chem.* **2000**, *158*, 389−393.
(41) Rodriguez-Gomez, A.; Holgado, J. P.; Caballero, A. Cobalt Carbide Identified as Catalytic Site for the Dehydrogenation of Ethanol to Acetaldehyde. *ACS Catal.* **2017**, *7*, 5243−5247.
(42) Gnanamani, M. K.; Jacobs, G.; Graham, U. M.; Ribeiro, M. C.; Noronha, F. B.; Shafer, W. D.; Davis, B. H. Influence of carbide formation on oxygenates selectivity during Fischer−Tropsch synthesis over Ce-containing Co catalysts. *Catal. Today* **2016**, *261*, 40−47.
(43) Anton, J.; Nebel, J.; Song, H.; Froese, C.; Weide, P.; Ruland, H.; Muhler, M.; Kaluza, S. The effect of sodium on the structure-activity relationships of cobalt-modified Cu/ZnO/Al2O3catalysts applied in the hydrogenation of carbon monoxide to higher alcohols. *J. Catal.* **2016**, *335*, 175−186.
(44) Xiang, Y.; Chitry, V.; Liddicoat, P.; Felfer, P.; Cairney, J.; Ringer, S.; Kruse, N. Long-chain terminal alcohols through catalytic CO hydrogenation. *J. Am. Chem. Soc.* **2013**, *135*, 7114−7117.
(45) Dong, W.; Liu, J.; Zhu, H.; Ding, Y.; Pei, Y.; Liu, J.; Du, H.; Jiang, M.; Liu, T.; Su, H.; Li, W. Co−Co2C and Co−Co2C/AC Catalysts for Hydroformylation of 1-Hexene under Low Pressure: Experimental and Theoretical Studies. *J. Phys. Chem. C* **2014**, *118*, 19114−19122.
(46) Xiang, Y.; Kruse, N. Tuning the catalytic CO hydrogenation to straight- and long-chain aldehydes/alcohols and olefins/paraffins. *Nat. Commun.* **2016**, *7*, 13058.
(47) Zhong, L.; Yu, F.; An, Y.; Zhao, Y.; Sun, Y.; Li, Z.; Lin, T.; Lin, Y.; Qi, X.; Dai, Y.; Gu, L.; Hu, J.; Jin, S.; Shen, Q.; Wang, H. Cobalt carbide nanoprisms for direct production of lower olefins from syngas. *Nature* **2016**, *538*, 84−87.
(48) Li, Z.; Lin, T.; Yu, F.; An, Y.; Dai, Y.; Li, S.; Zhong, L.; Wang, H.; Gao, P.; Sun, Y.; He, M. Mechanism of the Mn Promoter via CoMn Spinel for Morphology Control: Formation of Co2C Nanoprisms for Fischer−Tropsch to Olefins Reaction. *ACS Catal.* **2017**, *7*, 8023−8032.
(49) An, Y.; Zhao, Y.; Yu, F.; Lin, T.; Lu, Y.; Li, S.; Li, Z.; Dai, Y.; Wang, X.; Wang, H.; Zhong, L.; Sun, Y. Morphology control of Co2C nanostructures via the reduction process for direct production of lower olefins from syngas. *J. Catal.* **2018**, *366*, 289−299.
(50) An, Y.; Lin, T.; Yu, F.; Yang, Y.; Zhong, L.; Wu, M.; Sun, Y. Advances in direct production of value-added chemicals via syngas conversion. *Sci. China: Chem.* **2017**, *60*, 887−903.
(51) Dai, Y.; Zhao, Y.; Lin, T.; Li, S.; Yu, F.; An, Y.; Wang, X.; Xiao, K.; Sun, F.; Jiang, Z.; Lu, Y.; Wang, H.; Zhong, L.; Sun, Y. Particle Size Effects of Cobalt Carbide for Fischer−Tropsch to Olefins. *ACS Catal.* **2019**, *9*, 798−809.
(52) Li, Z.; Zhong, L.; Yu, F.; An, Y.; Dai, Y.; Yang, Y.; Lin, T.; Li, S.; Wang, H.; Gao, P.; Sun, Y.; He, M. Effects of Sodium on the Catalytic Performance of CoMn Catalysts for Fischer−Tropsch to Olefin Reactions. *ACS Catal.* **2017**, *7*, 3622−3631.
(53) An, Y.; Lin, T.; Yu, F.; Wang, X.; Lu, Y.; Zhong, L.; Wang, H.; Sun, Y. Effect of reaction pressures on structure-performance of Co2C-based catalyst for syngas conversion. *Ind. Eng. Chem. Res.* **2018**, *57*, 15647−15653.
(54) Wang, B.; Liang, D.; Zhang, R.; Ling, L. Crystal Facet Dependence for the Selectivity of C2 Species over Co2C Catalysts in the Fischer−Tropsch Synthesis. *J. Phys. Chem. C* **2018**, *122*, 29249−29258.
(55) Zhang, R.; Wen, G.; Adidharma, H.; Russell, A. G.; Wang, B.; Radosz, M.; Fan, M. C2 Oxygenate Synthesis via Fischer−Tropsch Synthesis on Co2C and Co/Co2C Interface Catalysts: How To Control the Catalyst Crystal Facet for Optimal Selectivity. *ACS Catal.* **2017**, *7*, 8285−8295.
(56) Kresse, G.; Furthmüller, J. Efficient iterative schemes for ab initio total-energy calculations using a plane-wave basis set. *Phys. Rev. B: Condens. Matter Mater. Phys.* **1996**, *54*, 11169−11186.
(57) Kresse, G.; Furthmüller, J. Efficiency of ab-initio total energy calculations for metals and semiconductors using a plane-wave basis set. *Comput. Mater. Sci.* **1996**, *6*, 15−50.
(58) Kresse, G.; Joubert, D. From ultrasoft pseudopotentials to the projector augmented-wave method. *Phys. Rev. B: Condens. Matter Mater. Phys.* **1999**, *59*, 1758−1775.
(59) Perdew, J. P.; Burke, K.; Ernzerhof, M. Generalized gradient approximation made simple. *Phys. Rev. Lett.* **1996**, *77*, 3865−3868.
(60) Zhao, Y. H.; Su, H. Y.; Sun, K.; Liu, J.; Li, W. X. Structural and electronic properties of cobalt carbide Co2C and its surface stability: Density functional theory study. *Surf. Sci.* **2012**, *606*, 598−604.
(61) Sun, K.; Zhao, Y.; Su, H.-Y.; Li, W.-X. Force reversed method for locating transition states. *Theor. Chem. Acc.* **2012**, *131*, 1118.
(62) Henkelman, G.; Jónsson, H. Improved tangent estimate in the nudged elastic band method for finding minimum energy paths and saddle points. *J. Chem. Phys.* **2000**, *113*, 9978−9985.
(63) Henkelman, G.; Uberuaga, B. P.; Jónsson, H. A climbing image nudged elastic band method for finding saddle points and minimum energy paths. *J. Chem. Phys.* **2000**, *113*, 9901−9904.
(64) Li, W. X.; Stampfl, C.; Scheffler, M. Why is a Noble Metal Catalytically Active? The Role of the O-Ag Interaction in the Function of Silver as an Oxidation Catalyst. *Phys. Rev. Lett.* **2003**, *90*, 256102.
(65) Reuter, K.; Scheffler, M. First-Principles Atomistic Thermodynamics for Oxidation Catalysis: Surface Phase Diagrams and Catalytically Interesting Regions. *Phys. Rev. Lett.* **2003**, *90*, 046103.
(66) Zhao, S.; Liu, X. W.; Huo, C. F.; Li, Y. W.; Wang, J.; Jiao, H. Surface Morphology of Hägg Iron Carbide (χ-Fe5C2) from Ab Initio Atomistic Thermodynamics. *J. Catal.* **2012**, *294*, 47−53.
(67) Reuter, K.; Scheffler, M. Composition, structure, and stability of RuO2(110) as a function of oxygen pressure. *Phys. Rev. B: Condens. Matter Mater. Phys.* **2001**, *65*, 035406.
(68) Zhao, S.; Liu, X.-W.; Huo, C.-F.; Li, Y.-W.; Wang, J.; Jiao, H. Determining surface structure and stability of ϵ-Fe2C, χ-Fe5C2, θ-Fe3C and Fe4C phases under carburization environment from combined DFT and atomistic thermodynamic studies. *Catal. Struct. React.* **2015**, *1*, 44−60.
(69) De Smit, E.; Cinquini, F.; Beale, A. M.; Safonova, O. V.; Van Beek, W.; Sautet, P.; Weckhuysen, B. M. Stability and Reactivity of ϵ-χ-θ Iron Carbide Catalyst Phases in Fischer−Tropsch Synthesis: Controlling μC. *J. Am. Chem. Soc.* **2010**, *132*, 14928−14941.
(70) Corral Valero, M.; Raybaud, P. Stability of carbon on cobalt surfaces in Fischer−Tropsch reaction conditions: A DFT study. *J. Phys. Chem. C* **2014**, *118*, 22479−22490.

DOI: 10.1021/acscatal.9b00649
ACS Catal. 2019, 9, 8093−8103

(71) Wulff, G. Zur Frage der Geschwindigkeit des Wachstums und der Auflösung der Krystallflagen. *Z. Kristallogr. - Cryst. Mater.* **1901**, *34*, 449−530.
(72) Momma, K.; Izumi, F. VESTA 3 for three-dimensional visualization of crystal, volumetric and morphology data. *J. Appl. Crystallogr.* **2011**, *44*, 1272−1276.
(73) Shetty, S.; Jansen, A. P. J.; Van Santen, R. A. Direct versus Hydrogen-Assisted CO Dissociation. *J. Am. Chem. Soc.* **2009**, *131*, 12874−12875.
(74) Filot, I. A. W.; Shetty, S. G.; Hensen, E. J. M.; Van Santen, R. A. Size and topological effects of rhodium surfaces, clusters and nanoparticles on the dissociation of CO. *J. Phys. Chem. C* **2011**, *115*, 14204−14212.
(75) Huo, C. F.; Li, Y. W.; Wang, J.; Jiao, H. Insight into CH4 Formation in Iron-Catalyzed Fischer−Tropsch Synthesis. *J. Am. Chem. Soc.* **2009**, *131*, 14713−14721.
(76) Ioffe, M. S.; Pollington, S. D.; Wan, J. K. S. High-Power Pulsed Radio-Frequency and Microwave Catalytic Processes: Selective Production of Acetylene from the Reaction of Methane over Carbon. *J. Catal.* **1995**, *151*, 349−355.
(77) Lebarbier, V. M.; Mei, D.; Kim, D. H.; Andersen, A.; Male, J. L.; Holladay, J. E.; Rousseau, R.; Wang, Y. Effects of La2O3 on the mixed higher alcohols synthesis from syngas over co catalysts: A combined theoretical and experimental study. *J. Phys. Chem. C* **2011**, *115*, 17440−17451.
(78) Zhao, Z.; Lu, W.; Zhu, H.; Dong, W.; Lyu, Y.; Liu, T.; Chen, X.; Wang, Y.; Ding, Y. Tuning the Fischer−Tropsch reaction over CoxMnyLa/AC catalysts toward alcohols: Effects of La promotion. *J. Catal.* **2018**, *361*, 156−167.
(79) Pei, Y.; Ding, Y.; Zhu, H.; Zang, J.; Song, X.; Dong, W.; Wang, T.; Yan, L.; Lu, Y. Study on the effect of alkali promoters on the formation of cobalt carbide (Co2C) and on the performance of Co2C via CO hydrogenation reaction. *React. Kinet., Mech. Catal.* **2014**, *111*, 505−520.
(80) Gnanamani, M. K.; Jacobs, G.; Shafer, W. D.; Sparks, D. E.; Hopps, S.; Thomas, G. A.; Davis, B. H. Low temperature water-gas shift reaction over alkali metal promoted cobalt carbide catalysts. *Top. Catal.* **2014**, *57*, 612−618.
(81) Du, H.; Zhu, H.; Chen, X.; Dong, W.; Lu, W.; Luo, W.; Jiang, M.; Liu, T.; Ding, Y. Study on CaO-promoted Co/AC catalysts for synthesis of higher alcohols from syngas. *Fuel* **2016**, *182*, 42−49.
(82) Jiao, G.; Ding, Y.; Zhu, H.; Li, X.; Li, J.; Lin, R.; Dong, W.; Gong, L.; Pei, Y.; Lu, Y. Effect of La2O3doping on syntheses of C1-C18mixed linear α-alcohols from syngas over the Co/AC catalysts. *Appl. Catal., A* **2009**, *364*, 137−142.
(83) Wang, Z.; Kumar, N.; Spivey, J. J. Preparation and characterization of lanthanum-promoted cobalt-copper catalysts for the conversion of syngas to higher oxygenates: Formation of cobalt carbide. *J. Catal.* **2016**, *339*, 1−8.
(84) Mohandas, J. C.; Gnanamani, M. K.; Jacobs, G.; Ma, W.; Ji, Y.; Khalid, S.; Davis, B. H. Fischer−Tropsch Synthesis: Characterization and Reaction Testing of Cobalt Carbide. *ACS Catal.* **2011**, *1*, 1581−1588.

DOI: 10.1021/acscatal.9b00649
ACS Catal. 2019, 9, 8093−8103